Journal of Materials Chemistry A

Accepted Manuscript

ROYAL SOCIETY OF CHEMISTRY

www.rsc.org/materialsA

Journal Name

ARTICLE

A $H_5BW_{12}O_{40}$-polyvinyl alcohol polymer electrolyte and its application in solid supercapacitors

Received 00th January 20xx,
Accepted 00th January 20xx

DOI: 10.1039/x0xx00000x

www.rsc.org/

Han Gao† and Keryn Lian*

A polymer electrolyte comprised of $H_5BW_{12}O_{40}$ (BWA) and cross-linked polyvinyl alcohol (BWA-XLPVA) has been developed and characterized for solid supercapacitors. The performance of this polymer electrolyte was compared to a known polymer electrolyte based on $H_4SiW_{12}O_{40}$ (SiWA). An enhanced proton conductivity was observed for BWA-XLPVA compared to its SiWA counterpart, especially under low humidity conditions (5% RH). Dielectric analyses revealed an increase of proton density and proton mobility in the BWA-based electrolyte. Solid-state ^{1}H NMR study showed that all protons in the BWA-based electrolyte were hydrated at the low humidity environment. This indicated that BWA had more crystallized water content than SiWA, resulting in higher proton mobility in the PVA matrix. An in-situ tracking of electrode potential in solid supercapacitors was utilized to identify the reactions and the factors limiting solid supercapacitor cell voltage for both BWA- and SiWA-based polymer electrolyte systems. A solid device leveraging the BWA-based polymer electrolyte achieved a cell voltage of 1.3 V, 0.2 V wider than a SiWA-based device.

Introduction

In conventional supercapacitors, ion-permeable and electrically insulating separator films are sandwiched between electrodes soaked with a liquid electrolyte.[1-8] Since leakage of the liquid electrolyte is a potential safety issue, especially when the material is environmentally hazardous, efforts abound to replace them with polymer electrolytes for next-generation solid supercapacitors that are not only safer, but also offer high performance, light weight, and flexible form factors.[9-12]

An ideal polymer electrolyte for supercapacitors should exhibit the following properties: (a) high ionic conductivity for high power output; (b) good ion accessibility at the electrode/electrolyte interface for high capacitance; (c) a wide electrochemical stability window for maximum cell voltage; and (d) high environmental and temperature stability for device safety and long service life. Polymer-in-salt electrolytes have shown promising performance, for the development of solid-state proton conductors. The major content of a polymer-in-salt electrolyte is a solid ionic conductor embedded in a polymer matrix. Because of the small polymer content, the ionic conduction mechanism depends on the solid "salt" and often obeys Arrhenius-type dependence.

Keggin-type Heteropolyacids (HPAs) are hydrous salts exhibiting the highest proton conductivity at room temperature among inorganic solid-state proton conductors.[13-19] They belong to a large family of metal-oxygen clusters of the early transition metals formulated as $H_z[X^{n+}M_{12}O_{40}]^{(8-n)-}$, where M is the addenda atom and X is the heteroatom.[17-21] $H_3PW_{12}O_{40}$ (PWA) and $H_4SiW_{12}O_{40}$ (SiWA) have shown excellent performance for liquid electrolytes[22, 23] and solid polymer electrolytes.[24, 25] Polymer electrolytes based on SiWA have demonstrated higher ambient proton conductivity and environmental stability than conventional perfluorosulphonic acids (e.g. Nafion®), sulfonated hydrocarbons, or acidic hydrogels (e.g. H_3PO_4-PVA).[12] Recently, we have synthesized and characterized aqueous $H_5BW_{12}O_{40}$ (BWA) as liquid electrolyte for supercapacitors.[26] BWA not only exhibited higher ionic conductivity than SiWA but it also had a 200 mV wider potential window when used as a liquid electrolyte.

To understand the feasibility of integrating BWA in polymer electrolytes, an electrolyte based on BWA and polyvinyl alcohol (PVA) was developed and investigated in terms of its proton conductivity and dielectric properties and compared to its known SiWA counterpart. Solid supercapacitor cells were demonstrated leveraging this polymer electrolyte. An in-situ electrode potential tracking method was utilized to monitor the individual potential changes in both positive and negative electrodes of the supercapacitors in the solid-state. In this paper, we report: (a) the mechanism and attributes for proton conductivity of a BWA-based polymer electrolyte; and (b) the potential window of the BWA-based polymer electrolyte and its interactions with the supercapacitor electrodes in solid cells.

Experimental

Department of Materials Science and Engineering, University of Toronto, Toronto, Ontario, Canada M5S 3E4
† Present address: Chemical Sciences and Engineering Division, Argonne National Laboratory, IL, USA.
* E-mail: keryn.lian@utoronto.ca

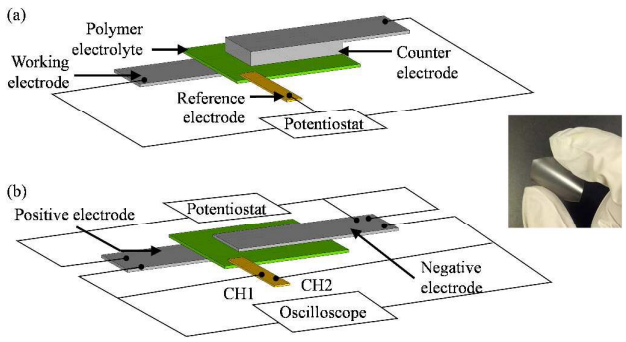

Figure 1 – Schematic diagrams of (a) 3-electrode system for single electrode characterization and (b) 2-electrode system for supercapacitor device characterization with in-situ potential tracking (the inset shows a photo of a polymer electrolyte film).

Preparation of polymer electrolytes

SiWA was purchased from Alfa Aesar and used as-received. The process of synthesizing BWA have been reported.[26] Both BWA and SiWA were blended in a cross-linked polymer matrix (XLPVA), which was prepared by mixing a 5 wt.% PVA (MW=145000, Sigma Aldrich) aqueous solution with glutaraldehyde ($CH_2(CH_2CHO)_2$, Alfa Aesar). The molar ratio of glutaraldehyde to PVA repeating unit was controlled at 0.013.[27] Both BWA- and SiWA-based electrolytes had a composition of ca. 90 wt% HPA and ca. 10 wt% XLPVA, assuming that most of the free water was removed in the drying process. Free-standing electrolyte films were obtained by solution-casting of the precursor solutions on polytetrafluoroethylene (PTFE) plates and dried under ambient conditions.

Construction of solid cells

Metallic cells for examining proton conductivity and dielectric characterizations were constructed by sandwiching a cast polymer electrolyte film between two stainless steel electrodes under 20 to 30 kPa pressure to form a two-electrode cell (stainless steel/polymer electrolyte/stainless steel). The geometric area of the electrodes was 1 cm^2. Ti or stainless steel spacers (100-250 µm thick) were used to obtain a consistent electrolyte thickness in the solid cells.

An aqueous-based graphite conductive ink (Alfa Aesar) was coated on thin stainless steel foils and dried in air as carbon electrodes for supercapacitor cells. The geometric area of the electrodes was 1 cm^2. Loading of graphite was ca. 5 $mgcm^{-2}$. Two different solid cells, a 3-electrode system (Figure 1a) and a 2-electrode system (Figure 1b), were used for single electrode characterization and device characterization, respectively.

Solid carbon cells were assembled in the following steps: (i) casting a free-standing polymer electrolyte film (2 x 2 cm) described above; (ii) coating the graphite electrodes with the electrolyte precursor solution via solution casting; (iii) cutting Ag pseudo-reference electrodes from screen-printed electrodes (Zensor R&D) and attaching them firmly to the polymer electrolyte film; (iv) assembling cells by sandwiching the free-standing electrolyte film with the reference electrode between the two graphite electrodes from step (ii) for 20 min under 20 to 30 kPa pressure at ambient temperature (Figure 1).

The difference between the "3-electrode" cell and the "2-electrode" cell was in the capacitance of the counter electrode. An electrode with the same graphite material but with much higher mass loading (ca. 20 $mgcm^{-2}$) was used in a 3-electrode cell for single electrode characterization (Figure 1a), while electrodes with identical graphite loadings were used as positive and negative electrodes to mimic a 2-electrode cell for supercapacitor device characterization (Figure 1b). An external reference electrode was connected to the 2-electrode cells to track the potential of both electrodes in solid supercapacitor devices.

Storage of polymer electrolytes and cells

All polymer electrolytes and the enabled-solid cells were stored under controlled conditions. The equilibrated relative humidity (RH) at 25 °C was controlled to emulate different environments (Table 1).[28] The three RH levels were chosen to represent conditions with stable and repeatable values in an ambient environment. Prior to performing measurements, the solid cells were kept in the desired RH for at least 15 days to reach equilibrium, unless otherwise specified. A temperature/humidity chamber (Espec SH-241) was used to conduct tests at different temperature and humidity level.

Electrochemical characterizations

All solid cells were characterized using cyclic voltammetry (CV) and electrochemical impedance spectroscopy (EIS). CV was performed either on a CHI 760D bipotentiostat or an EG&G PAR 263A potentiostat/galvanostat. EIS was performed on a Solartron 1255 frequency response analyzer interfaced with the EG&G 263A. The EIS spectra were recorded from 100 kHz to 1 Hz with 5 mV amplitude under zero voltage bias. Unless otherwise specified, all electrochemical experiments were carried out at room temperature.

For the 2-electrode cells, a DGS-122 digital oscilloscope was used to simultaneously track the change of both positive and negative electrode potentials against the pseudo-reference electrode during CV scans. Both potentiostat and oscilloscope were in a "floating" state for these measurements. The voltammogram of the supercapacitor cells and the corresponding potential tracking curves were obtained at the tenth CV cycle after reaching the steady state of both positive and negative electrode potentials. All solid 3-electrode and 2-electrode cells were stored at 75% RH overnight before any electrochemical tests to achieve steady-state conditions for ion conduction and at the electrode/electrolyte interfaces.

Dielectric characterizations of polymer electrolytes

Dielectric measurements of the metallic cells were carried out from -30 to 50 °C with a 10 °C interval. A 30 min equilibrium time was used at each temperature. The frequency-dependent response of an electrolyte is measured in complex impedance (Z*) and permittivity (ε*), which reflect the motion of mobile ions and dipoles.[29] The key parameters of interest are: proton conductivity (σ), dielectric constant (ε_r'), dielectric time constant (τ), free proton density (p_0), and mobility (µ). The solid sandwich cell can be considered as a capacitor such that the real part of the capacitance (C') can be extracted using its

impedance data.[30] The dielectric constant (ε_r') is extracted using

Table 1: Shelf storage conditions at room temperature.

RH	Controlled by	Comment
75 (±3)%	saturated NaCl solution	High humidity condition
45 (±3)%	saturated K_2CO_3 solution	Normal humidity condition
5 (±2)%	dried silica gel	Extremely low humidity condition

$$\varepsilon_r' = \frac{C'}{C_0} = \frac{-Z''}{2\pi f|Z|^2} \times \frac{d}{\varepsilon_0 A} \quad (1)$$

where Z is the complex impedance, Z" is the imaginary part of the complex impedance, d is the electrolyte thickness, and A is the electrode area. The dielectric loss (ε_r'') can be determined from

$$\varepsilon_r'' = (\varepsilon_r') \times (-\frac{1}{\tan\theta}) \quad (2)$$

where θ is the phase angle (or phase shift) of the metallic cell.

The Macdonald and Coelho model (a single ion approach) was used to deconvolute the different contributions to proton conductivity under the presence of electrode polarization.[31-34] The free ions in the polymer electrolyte were assumed to be protons due to the high Keggin HPA content and the immobile HPA anions. The proton transference number in HPAs is close to unity, which is also true for the polymer electrolytes. The free proton density, p_0, can then be obtained by

$$P_0 = \frac{4\tau_{EP}^2 kT\sigma}{q^2 d^2 \tau_s} \quad (3)$$

where k is Boltzmann's constant, q is elementary charge, and T is temperature. Here τ_{EP} is the dielectric time constant with electrode polarization at low frequencies while τ_s is the static dielectric time constant at high frequencies. τ is directly related to the dielectric constant and dc conductivity

$$\tau_{EP} = \frac{\varepsilon_{r,EP}\varepsilon_0}{\sigma} \quad (4)$$

$$\tau_s = \frac{\varepsilon_{r,s}\varepsilon_0}{\sigma} \quad (5)$$

where $\varepsilon_{r,s}$ and $\varepsilon_{r,EP}$ are the static dielectric constant and low frequency dielectric constant, respectively. Arrhenius relation was used to describe proton density and proton conductivity at different temperatures:

$$A_0 = A_\infty \exp(\frac{-E_a}{RT}) \quad (6)$$

where A_∞ is a pre-exponential factor, R is the gas constant, and E_a is the activation energy. Free proton density and mobility of the polymer electrolytes at low temperatures of -30 and -20 °C were directly calculated. At higher temperatures, the proton density was obtained by linear fitting using the Arrhenius relation, and mobility (μ) was calculated based on dc conductivity and free proton density:

$$\mu = \frac{\sigma}{qp_0} \quad (7)$$

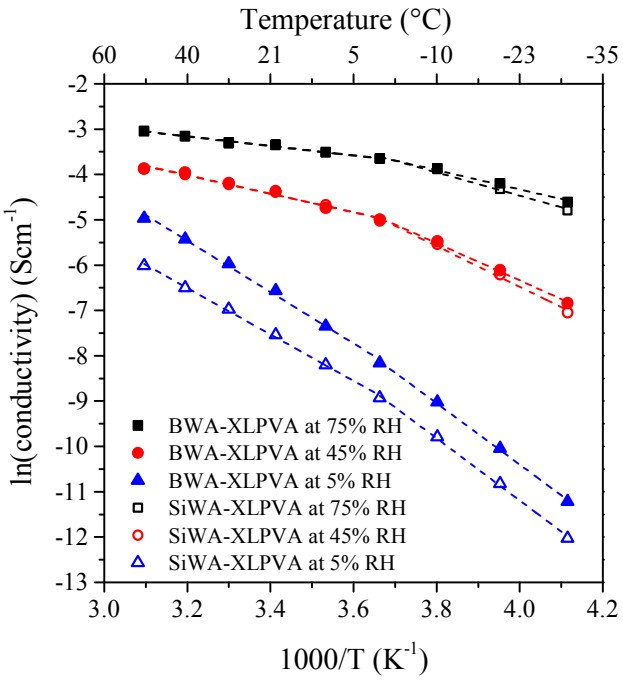

Figure 2 – Temperature dependence of proton conductivity for BWA-XLPVA and SiWA-XLPVA at 75%, 45%, and 5% RH from -30 to 50 °C.

Material characterizations

^{1}H solid-state nuclear magnetic resonance (NMR) spectra of a pre-dried (at ca. 5% RH) free-standing BWA-XLPVA film were recorded on an Agilent DD2-700 with the Larmor frequency 700 MHz and chemical shift has externally been referenced to tetramethylsilane (TMS). The ^{1}H NMR measurements have been taken as a function of temperature from -30 to 50 °C with a 10 °C interval.

Results and discussion

To study BWA and compare it with SiWA as a proton conductor in polymer electrolyte, the proton conductivity of the electrolytes was measured in a controlled environment. Dielectric properties were obtained and used to extract the free proton density and the mobility of both electrolytes from the obtained conductivity. The ^{1}H NMR spectra of BWA-XLPVA were analyzed to clarify the nature of protons in the polymer electrolyte. The potential window of both polymer electrolytes was studied utilizing an in-situ electrode potential tracking method in the solid-state.

Proton conductivity

A higher ionic conductivity of BWA over SiWA in the liquid solutions has been confirmed in a previous report.[26] In this work, we investigate the proton conductivity of these polymer electrolytes in the solid state. The high proton conductivity of HPAs results from the large number of crystallized water molecules in the HPA crystal hydrate, leading to a "quasi-liquid" state. However, the HPA crystals tend to dehydrate when heated or placed in a low RH atmosphere, resulting in a reduction in proton conductivity.[15] Therefore, a comparative

study of the conductivity of BWA-XLPVA and SiWA-XLPVA was performed at three RH levels: 75%, 45%, and 5% (Table 1). Arrhenius plots of proton conductivity (σ) for BWA-PVA and SiWA-PVA over a temperature range of -30 to 50 °C are shown in Figure 2 and the corresponding activation energy is summarized in Table 2.

Table 2: Proton conduction activation energies of BWA-XLPVA and SiWA-XLPVA at 75%, 45%, and 5% RH.

RH	Activation energy (kJmol^{-1})			
	BWA-XLPVA		SiWA-XLPVA	
	T>0 °C	T<0 °C	T>0 °C	T<0 °C
75%	8.7	17.7	8.7	21.3
45%	17.1	34.1	16.8	37.2
5%	47.0	56.3	42.5	57.0

The plots of proton conductivity in Figure 2 for both electrolytes can be divided into two regions: above and below 0 °C. The high linearity of the fitted lines in the two regions, opposed to the curved Arrhenius plots, suggested the conduction of protons via Grotthuss (i.e. hopping) mechanism. The activation energy was obtained from the slopes of the linearly fitted lines using Eq. 6 and increased with decreasing temperature (Table 2). Fast proton transportation within a polymer electrolyte is enabled by the rotation of crystallized water molecules in the HPA structure. The motion of water molecules is limited at temperatures below the water freezing point. This constitutes a higher energy barrier against structural reorganization/reorientation of water molecules and H^+-nH_2O clusters at low temperatures, limiting the proton conduction. In addition, the activation energy of both polymer electrolytes increased with dehydration (Table 2) in all temperature regions. This increase in the activation energy further confirmed the importance of water molecules in the polymer electrolytes. Not only the freezing of water molecules at low temperatures but also the removal of water molecules at low RH caused a discontinuity in the proton conduction path, resulting in a higher activation energy.

Further studies were focused on a comparison of the conductivity of BWA-XLPVA and SiWA-XLPVA. Both electrolytes exhibited similar proton conductivity at high and normal humidity conditions. For example, their conductivity at 20 °C was 35 mScm^{-1} (at 75% RH) and 13 mScm^{-1} (at 45% RH). At a higher temperature of 50 °C, proton conductivity increased to ca. 48 mScm^{-1} (at 75% RH) and 21 mScm^{-1} (at 45% RH). Due to the dehydration (i.e. loss of crystallized water molecules) in the HPA at 5% RH, both BWA-XLPVA and SiWA-XLPVA suffered from a reduction in conductivity. However, BWA-XLPVA demonstrated a roughly three times higher conductivity than SiWA-XLPVA, e.g. 1.4 vs. 0.5 mScm^{-1} at 20 °C and 7 vs. 2.5 mScm^{-1} at 50 °C. This enhancement in conductivity of BWA-PVA at such low humidity environment is beneficial, especially for thin and solid electrochemical devices that operate under ambient conditions with little or no packaging.

Dielectric characterizations

Since the effect of replacing SiWA with BWA on the proton conductivity of the polymer electrolytes was more pronounced at 5% RH (Figure 2), further comparative investigations based on ac impedance measurements were carried out under low humidity conditions to identify the origin of the difference in conductivity. Figure 3 shows the dielectric constant and dielectric loss of BWA-XLPVA and SiWA-XLPVA as a function of frequency at different temperatures.

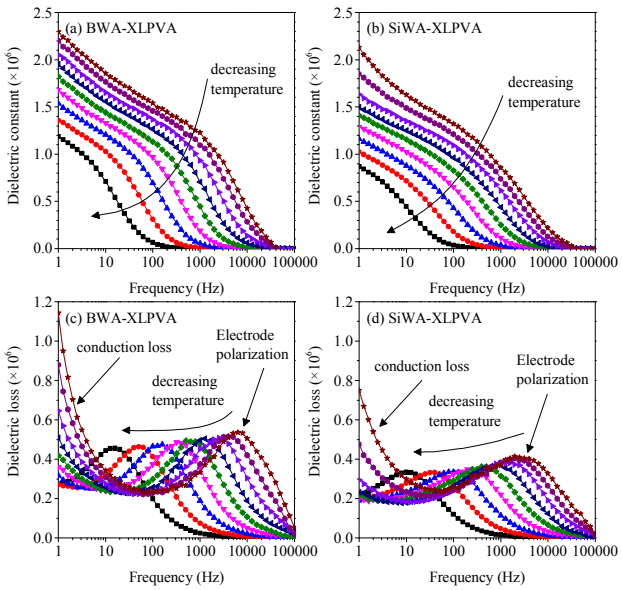

Figure 3 – Dielectric constant of (a) BWA-XLPVA, (b) SiWA-XLPVA, and dielectric loss of (c) BWA-XLPVA, (d) SiWA-XLPVA, from -30 to 50 °C.

Because of the low polymer content and limited chain movements in a polymer-in-salt electrolyte, polarization caused by polymer main chain and/or side chain motions are small and negligible. Therefore, the two dominating types of polarization are: (i) dipole polarization of HPA hydrates and PVA as well as interfacial polarization among these components at high frequencies; and (ii) electrode polarization (i.e. formation of an electric double-layer) at low frequencies. In Figure 3a and b, both polymer electrolytes showed a high apparent dielectric constant at low frequencies related to electrode polarization. As frequency increased, the dielectric constant decreased. The low frequency dielectric constant (e.g. at 1 Hz) of BWA-XLPVA was higher than that of SiWA-XLPVA, indicating a higher capacitance of the BWA-enabled cell. Also at any frequency, the dielectric constant decreased with the decrease of temperature.

In the dielectric loss vs. frequency plots (Figure 3c and d), peaks from both relaxation of electrode polarization (at high frequencies) and conduction loss (at low frequencies) were observed. Shifting of the electrode polarization peak with temperature was much more pronounced and the conduction loss peak only appeared partially. Shifting of the electrode polarization peak is due to a higher sensitivity of proton conductivity with temperature variation at this extremely dry condition while shifting of the conduction loss peak is a result of limited ion mobility. In both BWA-XLPVA and SiWA-XLPA, the frequency of the dielectric loss peak decreased with the decrease of temperature (Figure 3c and d). Although BWA-XLPVA exhibited higher magnitude of loss peak than SiWA-

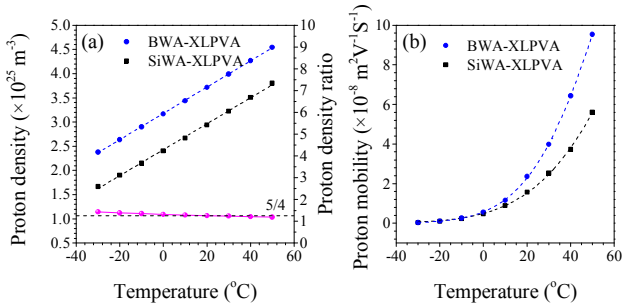

Figure 4 – (a) Proton density and (b) proton mobility of BWA-XLPVA and SiWA-XLPVA at 5% RH from -30 to 50 °C.

XLPVA due to its higher dielectric constant, BWA-XLPVA exhibited a faster response with shorter relaxation (i.e. peaks at higher frequency) when compared to SiWA-XLPVA at all temperatures, confirming the higher proton conductivity of BWA-XLPVA. In addition, due to the more conductive nature of BWA-XLPVA, the tail in its dielectric loss spectra occurred at -10 °C while the tail in the dielectric loss spectra of SiWA-XLPVA occurred at 10 °C.

Table 3: Protons density (p_0), mobility (μ), and conductivity (σ) of BWA-XLPVA and SiWA-XLPVA at 5% RH (Temperature = -30 and -20 °C).

T (°C)	Polymer electrolyte	p_0 (m^{-3})	μ ($m^2V^{-1}s^{-1}$)	σ ($mScm^{-1}$)
-30	BWA-XLPVA	2.38×10^{25}	3.53×10^{-10}	0.013
	SiWA-XLPVA	1.67×10^{25}	3.14×10^{-10}	0.006
-20	BWA-XLPVA	2.64×10^{25}	1.02×10^{-9}	0.043
	SiWA-XLPVA	1.91×10^{25}	9.15×10^{-10}	0.020

Using a single-ion approach as described in our pervious study,[29] proton densities were calculated as a function of temperature. To minimize the influence of self-resonance on the dielectric response of the polymer electrolytes, the dielectric constant at -30 and -20 °C was first analyzed. The proton density of each electrolyte was first calculated from the respective dielectric time constant (τ_s and τ_{EP}) using Eq. 3, where τ_s was related to the steady-state dielectric constant ($\varepsilon_{r,s}$) and τ_{EP} was related to the dielectric constant at 1 Hz ($\varepsilon_{r,EP}$). We started at a low temperature to minimize the influence of self-resonance at high frequencies. The calculated p_0 and μ at -30 and -20 °C are listed in Table 3.

The value of $\varepsilon_{r,s}$ is difficult to extract from Figure 3a and b at temperatures above -20 °C due to the lack of a clear plateau in the high frequency region of the dielectric constant plots. Thus, an indirect approach was used to calculate proton density leveraging the density at -30 and -20 °C (Table 3) and the Arrhenius relationship to obtain the proton density at temperatures from -20 to 50 °C (Figure 4a). This is because, at a low RH of 5%, the proton conductivity of both electrolytes was based on proton density rather than proton mobility. This is especially true at low temperatures. Since BWA ($H_5BW_{12}O_{40}$) has more protons than SiWA ($H_4SiW_{12}O_{40}$), the BWA-based electrolyte showed consistently higher proton density than that of its SiWA counterpart throughout the temperature range. The ratio of proton density shown in Figure 4a also agreed well with the theoretical value of 5/4.

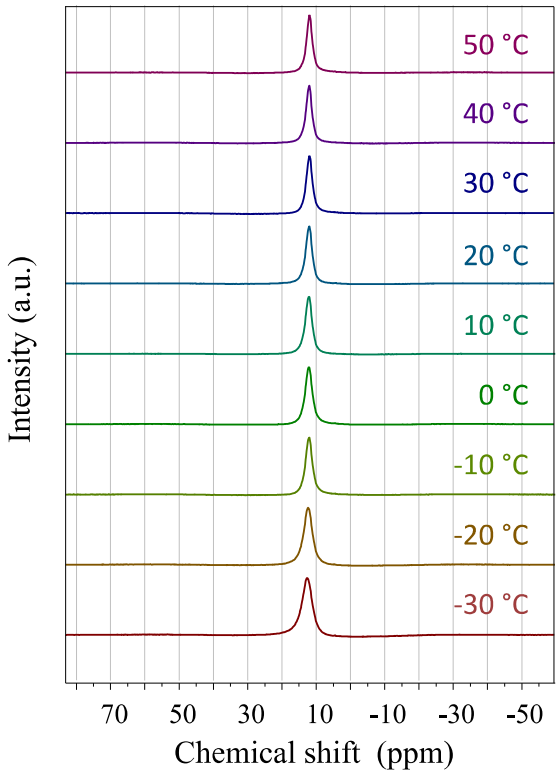

Figure 5 – Solid-state ^{1}H NMR spectra of BWA-XLPVA from -30 to 50 ° C (stored at 5% RH).

Proton mobility at 5% RH for BWA-XLPVA and SiWA-XLPVA was calculated based on proton conductivity and proton density using Eq. 7. Figure 4b depicts the mobility of both polymer electrolytes as a function of temperature. Both BWA-XLPVA and SiWA-XLPVA showed higher proton mobility with increased temperature. At low temperatures, while both electrolytes had very low proton mobility due to the freezing of water, BWA-XLPVA showed higher proton mobility than its SiWA counterpart at temperatures above 0 °C. A hypothesis was that BWA contained more water in this condition, facilitating proton transportation. Since at a low RH of 5%, all free water has likely been eliminated, the water in the electrolyte films was mainly from crystallized water molecules. It is well known that at low RH, SiWA forms hexahydrate, where three of its four protons are hydrated forming a protonated dimer $H_2O\cdots H^+\cdots OH_2$ (i.e. $H_5O_2^+$).[35-39] This results in a single isolated proton (i.e. non-hydrated proton) in SiWA. To gain an understanding of the level of hydration of BWA at low RH condition, the condition of protons in BWA should be compared to SiWA.

NMR characterization of polymer electrolytes

Different from impedance and dielectric analyses which focus on the dynamics of proton transportation in the long range order, solid-state ^{1}H NMR analysis provides a microscopic view on the short range localized motion of protons. Therefore, the nature of protons in BWA-XLPVA stored at 5% RH can be investigated and compared to available data describing isolated protons in dried HPAs (e.g. SiWA).[36, 40]

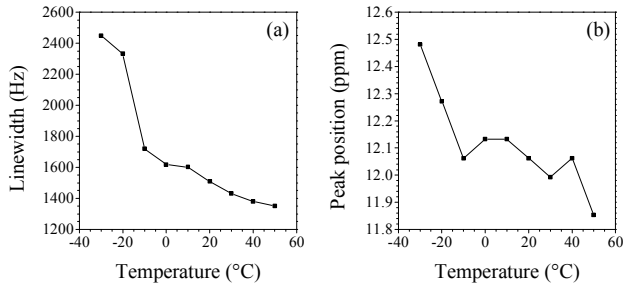

Figure 7 - (a) Solid-state ^{1}H NMR line width of BWA-XLPVA and (b) line position of BWA-XLPVA extracted from Figure 5.

Figure 5 shows the ^{1}H NMR spectra of BWA-XLPVA from -30 to 50 °C. The extracted peak width and peak position are shown in Figure 6. In Figure 5, relatively broad peaks (e.g. a few kHz wide) were observed at all temperatures, primarily due to the strong ^{1}H-^{1}H dipolar interactions in the electrolyte film. This peak broadening can be used as an indicator for proton mobility. At low temperatures, the peak width (defined as full width at half maximum) was broader (Figure 6a), implying that the protons were essentially immobile because of the strong dipole-dipole interaction. With an increase in temperature, the peak width decreased as a result of increased proton mobility. The proton mobility at higher temperatures was high enough to balance dipolar interactions, producing this peak narrowing effect (Figure 6a). The NMR results also supported the trend in proton mobility analyses depicted in Figure 4b.

Further investigations focused on the peak position to identify the origin of these peaks (Figure 6b). Typically the resonance (i.e. peak position) moves to lower frequencies with an increase in temperature as a result of the reduction in hydrogen bonding within the polymer electrolyte at elevated temperatures, where the hydrogen bonds begin to elongate and break. At room temperature (i.e. 20 °C), the proton chemical shift was ca. 12 ppm. It has been reported that the chemical shift of isolated protons in HPAs (including SiWA) is 9 ppm[36] and the predicted chemical shift of hydrated protons in the form of $H_5O_2^+$ and H_3O^+ is 10.6 and 13.4 ppm, respectively.[40] Therefore, the observed peak in Figure 6b could be regarded as a coalesced peak of H_3O^+ and $H_5O_2^+$. These results indicate that all protons in BWA-XLPVA were hydrated with no isolated protons. Since BWA ($H_5BW_{12}O_{40}$) has more protons associated with its anion than SiWA ($H_4SiW_{12}O_{40}$), BWA must contain more crystallized water molecules as well. Rashkin et. al. identified that dried BWA is present in the form of decahydrate ($H_5BW_{12}O_{40}\bullet 10\ H_2O$)[41] while the potassium salt of BWA contained eleven crystallized water molecules ($K_5BW_{12}O_{40}\bullet 11H_2O$).[42] Both cases support the notion that BWA possesses more crystallized water content than SiWA in dry conditions, resulting in a higher proton conductivity of BWA-XLPVA (Figure 2).

Analysis of operating cell voltage

Having confirmed that the higher proton conductivity of BWA-XLPVA resulted from its higher proton density and the larger amount of crystallized water molecules, BWA-XLPVA was studied as an electrolyte for solid supercapacitors and compared to a cell using SiWA-XLPVA. The electrochemical potential window of an electrolyte is an important property as it affects the operating cell voltage and thus energy density. Previously we have identified that an increased negative potential for the anion reaction in aqueous BWA led to a wider electrochemical stability window than for aqueous SiWA-based supercapacitors.[26] In this work, we used the same approach,

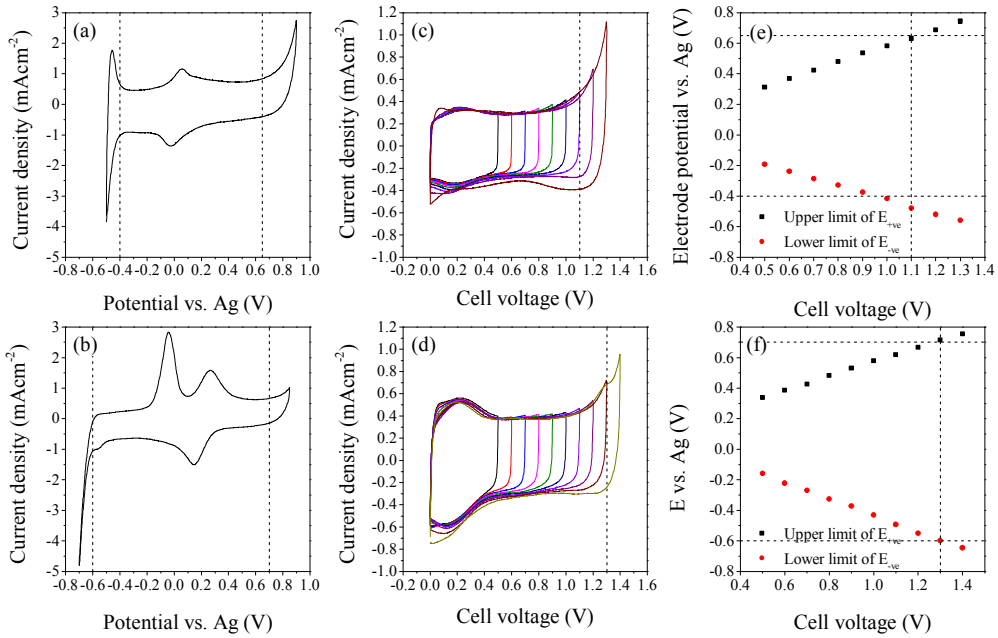

Figure 6 – 3 electrode CVs of graphite electrodes with (a) SiWA-XLPVA and (b) BWA-XLPVA (scan rate = 100 mVs^{-1}); CVs of (c) a SiWA-XLPVA-enabled and (d) a BWA-XLPVA-enabled solid graphite-graphite cell at incremental cell voltage (10th cycle, scan rate = 100 mVs^{-1}); electrode potential limits of both positive and negative electrodes as a function of cell voltage in the (e) SiWA-XLPVA-enabled and (f) BWA-XLPVA-enabled solid cells.

but in solid-state, to study the difference in potential window between the SiWA- and BWA-based polymer electrolytes as well as to understand the interactions between the polymer electrolytes and the electrodes in solid supercapacitors.

The electrochemical behavior of 3-electrode systems of both SiWA-XLPVA and BWA-XLPVA was first studied using CV and is depicted in Figure 7a and b. In this configuration, high graphite loading counter electrodes and external reference electrodes were used as shown in Figure 1b. In SiWA-XLPVA (Figure 7a), the open-circuit potential (OCP) of the graphite electrode with SiWA-XLPVA electrolyte was about 0 V. A pair of redox peaks from the carbon functional groups was also observed at around 0 V. The positive potential limit is about 0.65 V due to oxygen evolution, while the negative potential limit was -0.4 V and can be attributed to the reduction of WVI in $[SiW_{12}O_{40}]^{4-}$. The OCP of the graphite electrode with BWA-XLPVA was ca. 0.2 V (Figure 7b). A pair of redox peaks from the carbon functional groups was observed in the CV. The positive potential limit of the cell was about 0.7 V while the negative potential limit was -0.6 V due to hydrogen evolution. This extended negative potential limit agrees well with the difference between the onsets of the first electron reduction between BWA and SiWA in aqueous solutions [26]. A broad anodic peak related to the oxidation of hydrogen was observed at -0.1 V. Since the generation of hydrogen can only occur at potentials lower than -0.6 V the anodic peak will not affect the overall performance of the solid supercapacitor as long as the potential of the negative electrode does not exceed the limit of -0.6 V.

Further studies were performed using the 2-electrode system for SiWA-XLPVA and BWA-XLPVA. The CV profiles with incremental cell voltages are shown in Figure 7c and d. Both solid cells depict near-rectangular-shaped profiles, suggesting highly capacitive behavior. While the increased current density limited the maximum cell voltage of the SiWA-enabled supercapacitor to ca. 1.1 V, the cell voltage of the BWA-enabled supercapacitor had a maximum cell voltage of 1.3 V, 0.2 V wider than its SiWA counterpart.

During charging of a capacitor, the potentials of both electrodes move against each other and away from the OCP, reaching their respective potential limit. Figure 7e and f show the positive and negative potential limits of the two electrodes as a function of cell voltage for each solid supercapacitor. Also marked in Figure 7e and f are the onsets of the anion reduction reaction and oxygen evolution of SiWA or BWA obtained from Figure 7a and b. In Figure 7e, the negative electrode of the SiWA-enabled cell reached the reduction reaction of the SiWA anion at a cell voltage of 0.9 V. Further increase in cell voltage led to the positive electrode reaching the oxygen evolution potential and limited the maximum cell voltage to 1.1 V. In Figure 7f, both the negative and positive electrodes reached their limits simultaneously resulting in the maximum cell voltage of the BWA-enabled capacitor of 1.3 V. This further confirms the wider electrochemical potential window of BWA-XLPVA and the higher maximum cell voltage of the BWA-XLPVA-enabled solid supercapacitor. In our previous study, the BWA-based solid supercapacitor showed very stable performance with no significant decay in capacitance after being cycled for 5000 cycles.[26] The higher proton conductivity and wider electrochemical potential window of BWA-XLPVA suggest that this material is a very promising electrolyte for high-rate and high-power solid-state supercapacitors.

Conclusions

HPA-based polymer electrolytes demonstrate high solid-state proton conductivity (10^{-3} to 10^{-2} Scm^{-1}) at room temperature due to fast proton hopping through conduction networks. In this work, properties of BWA for a HPA-based polymer electrolyte were studied. BWA-XLPVA showed two major advantages over SiWA-XLPVA: (a) A higher proton conductivity at a low humidity environment; and (b) a wider electrochemical potential window.

The higher proton conductivity of BWA-XLPVA was attributed to its higher proton density and proton mobility through dielectric analysis. These properties were derived as a function of temperature using a single-ion approach. ^{1}H NMR results revealed that BWA contained more crystallized water molecules than SiWA, which resulted in higher proton mobility. An in-situ electrode potential tracking method unveiled an increased negative potential for the anion reaction in BWA, which led to a wider electrochemical stability window of BWA-XLPVA than for its SiWA counterpart. These properties of the BWA-based polymer electrolyte are highly desirable for high-rate and high power solid electrochemical energy storage devices.

Acknowledgements

We appreciate the financial support from NSERC Canada. H. Gao would like to acknowledge the NSERC Alexander Graham Bell Canada Graduate Scholarship and Hatch Graduate Scholarships for Sustainable Energy Research. We also thank Dr. Sergiy Nokhrin of the Department of Chemistry at University of Toronto for the help in solid-state NMR measurements.

References

1. B. E. Conway, *Electrochemical supercapacitors: scientific fundamentals and technological applications*, Springer, New York, 1999.
2. B. Conway and W. Pell, *J. Solid State Electrochem.*, 2003, **7**, 637-644.
3. A. Burke, *J. Power Sources*, 2000, **91**, 37-50.
4. *U.S. Pat.,* 2800616, 1957.
5. P. Simon and Y. Gogotsi, *Nature Mater.*, 2008, **7**, 845-854.
6. P. Simon and Y. Gogotsi, *Acc. Chem. Res.*, 2012, **46**, 1094-1103.
7. L. L. Zhang and X. S. Zhao, *Chem. Soc. Rev.*, 2009, **38**, 2520-2531.
8. M. Toupin, T. Brousse and D. Bélanger, *Chem. Mater.*, 2004, **16**, 3184-3190.

9. C. A. Nguyen, A. A. Argun, P. T. Hammond, X. Lu and P. S. Lee, *Chem. Mater.*, 2011, **23**, 2142-2149.
10. L.-Q. Fan, J. Zhong, J.-H. Wu, J.-M. Lin and Y.-F. Huang, *J. Mater. Chem. A*, 2014, **2**, 9011-9014.
11. B. D. Ghosh and J. E. Ritchie, *Chem. Mater.*, 2010, **22**, 1483-1491.
12. H. Gao and K. Lian, *RSC Adv.*, 2014, **4**, 33091-33113.
13. A. Hardwick, P. G. Dickens and R. C. T. Slade, *Solid State Ionics*, 1984, **13**, 345-350.
14. K. D. Kreuer, M. Hampele, K. Dolde and A. Rabenau, *Solid State Ionics*, 1988, **28–30, Part 1**, 589-593.
15. R. C. T. Slade, H. A. Pressman and E. Skou, *Solid State Ionics*, 1990, **38**, 207-211.
16. R. C. T. Slade, J. Barker and H. A. Pressman, *Solid State Ionics*, 1988, **28–30, Part 1**, 594-600.
17. U. B. Mioč, M. R. Todorović, M. Davidović, P. Colomban and I. Holclajtner-Antunović, *Solid State Ionics*, 2005, **176**, 3005-3017.
18. A. M. Herring, *J. Macromol. Sci., Polym. Rev.*, 2006, **46**, 245-296.
19. S. Sachdeva, J. Turner, J. Horan and A. Herring, in *Fuel Cells and Hydrogen Storage*, eds. A. Bocarsly and D. M. P. Mingos, Springer Berlin Heidelberg, 2011, vol. 141, ch. 45, pp. 115-168.
20. M. Sadakane and E. Steckhan, *Chem. Rev.*, 1998, **98**, 219-238.
21. D. E. Katsoulis, *Chem. Rev.*, 1998, **98**, 359-388.
22. K. Lian and C. Li, *Electrochem. Solid-State Lett.*, 2008, **11**, A158-A162.
23. K. Lian and C. M. Li, *Electrochem. Solid-State Lett.*, 2009, **12**, A10-A12.
24. H. Gao, Q. Tian and K. Lian, *Solid State Ionics*, 2010, **181**, 874-876.
25. H. Gao and K. Lian, *Electrochim. Acta*, 2010, **56**, 122-127.
26. H. Gao, A. Virya and K. Lian, *J. Mater. Chem. A*, 2015, **3**, 21511-21517.
27. H. Gao and K. Lian, *J. Mater. Chem.*, 2012, **22**, 21272.
28. A. Carotenuto and M. Dell'Isola, *Int. J. Thermophys.*, 1996, **17**, 1423-1439.
29. H. Gao and K. Lian, *ACS Appl. Mater. Interfaces*, 2013, **6**, 464-472.
30. P. L. Taberna, P. Simon and J. F. Fauvarque *J. Electrochem. Soc.*, 2003, **150**, A292-A300.
31. R. J. Klein, S. Zhang, S. Dou, B. H. Jones, R. H. Colby and J. Runt, *J. Chem. Phys.*, 2006, **124**, 144903.
32. J. R. Macdonald, *Phys. Rev.*, 1953, **92**, 4-17.
33. J. R. Macdonald, *J. Chem. Phys.*, 1974, **61**, 3977-3996.
34. R. Coelho, *J. Non-Cryst. Solids*, 1991, **131–133, Part 2**, 1136-1139.
35. G. M. Brown, M.-R. Noe-Spirlet, W. R. Busing and H. A. Levy, *Acta Crystallogr. Sect. B: Struct. Sci.*, 1977, **33**, 1038-1046.
36. S. Uchida, K. Inumaru and M. Misono, *J. Phys. Chem. B*, 2000, **104**, 8108-8115.
37. A. Bielański, J. Datka, B. Gil, A. Małecka-Lubańska and A. Micek-Ilnicka, *Catal. Lett.*, 1999, **57**, 61-64.
38. A. Bielański, A. Małecka-Lubańska, A. Micek-Ilnicka and J. Pożniczek, *Top. Catal.*, 2000, **11-12**, 43-53.
39. A. Bielański, J. Pożniczek and M. Hasik, *J. Therm. Anal.*, 1995, **44**, 717-723.
40. M. Krossner and J. Sauer, *J. Phys. Chem.*, 1996, **100**, 6199-6211.
41. J. A. Rashkin, E. D. Pierron and D. L. Parker, *J. Phys. Chem.*, 1967, **71**, 1265-1270.
42. A. R. Couto, C. N. Trovao, J. Rocha, A. M. V. Cavaleiro and J. D. P. de Jesus, *J. Chem. Soc., Dalton Trans.*, 1994, DOI: 10.1039/DT9940002585, 2585-2586.

Graphical abstract

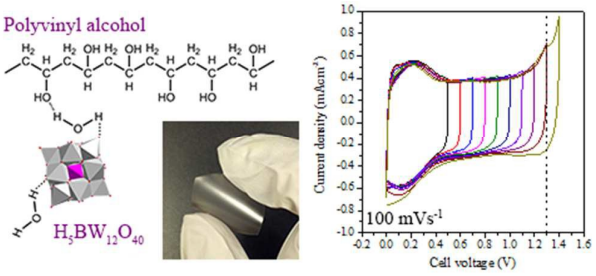

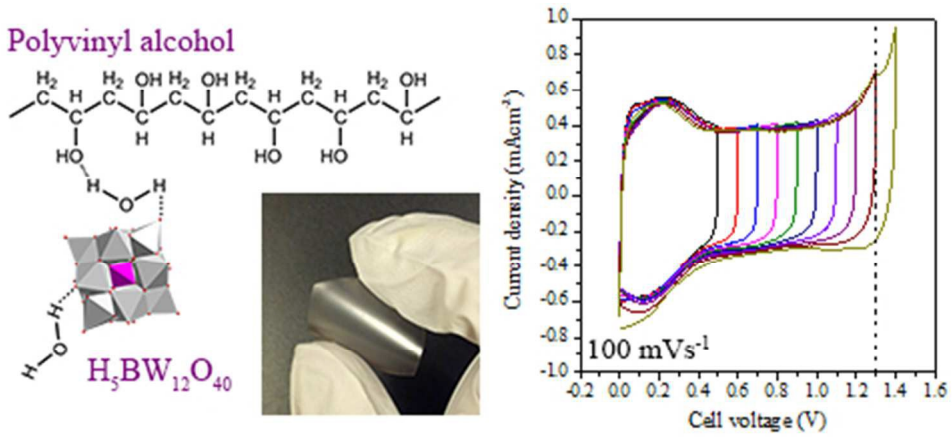

176x76mm (72 x 72 DPI)